LPT–Orsay 08/38
FTUAM 08/6
IFT-UAM/CSIC-08-21
IFT-6/2008

Determining the WIMP mass using the complementarity between direct and indirect searches and the ILC

N. Bernal[1], A. Goudelis[1],Y. Mambrini[2], C. Muñoz[3,4]

[1] Laboratoire de Physique Théorique, Université Paris-Sud, F-91405 Orsay, France

[2] Institute of Theoretical Physics, Warsaw University, ul. Hoza 69, 00-681 Warsaw, Poland

[3] Departamento de Física Teórica C-XI, Universidad Autónoma de Madrid, Cantoblanco, 28049 Madrid, Spain

[4] Instituto de Física Teórica UAM/CSIC, Universidad Autónoma de Madrid, Cantoblanco, 28049 Madrid, Spain

Abstract

We study the possibility of identifying dark matter properties from XENON–like 100 kg experiments and the GLAST satellite mission. We show that whereas direct detection experiments will probe efficiently light WIMPs, given a positive detection (at the 10% level for $m_\chi \lesssim 50$ GeV), GLAST will be able to confirm and even increase the precision in the case of a NFW profile, for a WIMP-nucleon cross-section $\sigma_{\chi-p} \lesssim 10^{-8}$ pb. We also predict the rate of production of a WIMP in the next generation of colliders (ILC), and compare their sensitivity to the WIMP mass with the XENON and GLAST projects.

Contents

1 Introduction

There exist strong evidences that a large fraction of the matter in our Universe is non-luminous [1]. Such evidences include the motion of cluster member galaxies [2], gravitational lensing [3], cosmic microwave background [4], observations of the flat rotation curves of galaxies [5], etc. Dark matter plays a central role in current structure formation theories, and its microscopic properties have significant impact on the spatial distribution of mass, galaxies and clusters. Unraveling the nature of the dark matter is therefore of critical importance. A Weakly Interacting Massive Particle (WIMP), with mass lying from the GeV to the TeV scale, is one of the preferred candidates for the dark matter of the Universe.

Different experimental programs are developing huge efforts to observe and identify the particle nature of the dark matter. This can be achieved by direct measurement of the recoil energy of a nucleus by a WIMP, or indirectly via the observation of WIMP annihilation products. In both cases, the sensitivity depends strongly on the background and on the theoretical assumptions of the model. It would be interesting to combine all these efforts to invent intelligent strategies for determining the nature of dark matter [6]. Recently, several works (see Refs. [7] and [8] for the case of direct and indirect detection respectively) have shown that precision measurements of the mass of the WIMP are not only reserved to the domain of accelerator physics. In all these studies, model independent bounds are derived for annihilation cross-sections, masses or WIMP–nucleus scattering cross-sections. The drawback of a model-independent framework (lack of determined microscopic processes) is largely compensated by the universality of the method: instead of restricting a theoretical parameter space, we restrict physical observable quantities (masses, branching ratios). Indeed, these limits are valid for all candidates for WIMPs, such as for example the supersymmetric neutralino, the lightest Kaluza Klein excitation, etc.

The aim of the present work is to analyse two of the most promising experiments, XENON [9] and GLAST [10], calculating and comparing their sensitivity to a WIMP mass depending on the astrophysical hypothesis (velocity distribution of WIMPs, density profile of the galactic halo). In addition, using the known cosmological abundance of dark matter in the Universe, we predict the radiative WIMP production rate in the next generation of colliders (ILC) and compare their sensitivity to the WIMP mass with the XENON and GLAST projects. The paper is organised as follows. In section 2 we discuss the event rate and WIMP-nucleon scattering cross-section for a XENON-like experiment, in a complete microscopic model-independent approach. In Section 3 we carry out a similar analysis for the GLAST experiment, discussing in this case the WIMP annihilation cross section, and taking into account different halo profiles. Section 4 is dedicated to the comparison between these two modes of detection. In Section 5 we analyse the sensitivity that we can expect in such a model-independent framework for a linear collider. Finally, in Section 6 we carry out the comparison between the three detection modes. The conclusions are left for Section 7.

2 Direct detection

2.1 Differential event rate

In spite of the experimental challenges, a number of efforts worldwide are actively pursuing to directly detect WIMPs with a variety of targets and approaches. Many direct dark matter detection experiments are now either operating or in preparation. All these experiments

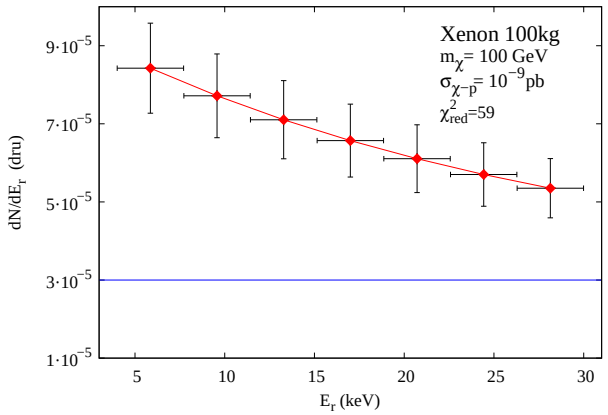

Figure 1: XENON expectations for event rate in the case of a WIMP mass $m_\chi = 100$ GeV and cross section $\sigma_{\chi-p} = 10^{-9}$ pb. The error bars shown are those expected for the XENON 100 kg experiment after 3 years of observation. The lower (blue) line is the background–only prediction. The χ^2 per degree of freedom ($\chi^2_{\rm red}$) is 59, giving a signal clearly distinguishable from the background.

measure the number N of elastic collisions between WIMPs and target nuclei in a detector, per unit detector mass and per unit of time, as a function of the nuclear recoil energy E_r. The detection rate in a detector depends on the density $\rho_0 \simeq 0.3$ GeV cm^{-3} and velocity distribution $f(v_\chi)$ of WIMPs near the Earth. In general, the differential rate per unit detector mass and per unit of time can be written as:

$$\frac{dN}{dE_r} = \frac{\sigma_{\chi-N}\,\rho_0}{2\,m_r^2\,m_\chi}\,F(E_r)^2 \int_{v_{min}(E_r)}^{\infty} \frac{f(v_\chi)}{v_\chi} dv_\chi \ , \tag{2.1}$$

where the WIMP-nucleus cross section, $\sigma_{\chi-N}$, is related to the WIMP-nucleon cross section, $\sigma_{\chi-p}$, by $\sigma_{\chi-N} = \sigma_{\chi-p}(A m_r/M_r)^2$, with $M_r = \frac{m_\chi m_p}{m_\chi+m_p}$ the WIMP-nucleon reduced mass, $m_r = \frac{m_\chi m_N}{m_\chi+m_N}$ the WIMP-nucleus reduced mass, m_χ the WIMP mass, m_N the nucleus mass, and A the atomic weight. F is the form factor.

For the velocity distribution we take a simple Maxwellian halo

$$f(v_\chi)\,d^3v_\chi = \frac{1}{(v_\chi^0)^3\pi^{3/2}}\,e^{-(v_\chi/v_\chi^0)^2}\,d^3v_\chi \ , \tag{2.2}$$

where $v_\chi^0 \simeq 220$ km/s is the velocity of the Sun around the galactic center, and we have neglected the motion of the Earth around the Sun. After integrating over the angular part in order to find the speed distribution we get:

$$f(v_\chi)\,dv_\chi = \frac{4\,v_\chi^2}{(v_\chi^0)^3\sqrt{\pi}}\,e^{-(v_\chi/v_\chi^0)^2}\,dv_\chi \ , \tag{2.3}$$

The integration over velocities is limited to those which can give place to a recoil energy E_r, thus there is a minimal velocity given by $v_{min}(E_r) = \sqrt{\frac{m_N\,E_r}{2\,m_r^2}}$.

The effective interaction between the WIMP and a nucleus is given by the Woods-Saxon form factor

$$F(E_r) = \frac{3\,j_1(q\,R_1)}{q\,R_1}\,e^{-(q\,s)^2} \ , \tag{2.4}$$

where the transferred momentum is $q = \sqrt{2\, m_N\, E_r}$, j_1 is a spherical Bessel function, $R_1 = \sqrt{R^2 - 5\, s^2}$ with $R \simeq 1.2 \cdot A^{1/3}$ fm, A the mass number, and $s \simeq 1$ fm.

In order to compare the theoretical signal with the background it is necessary to calculate the χ^2. Let us call N^{sign} the signal, N^{bkg} the background and $N^{tot} = N^{sign} + N^{bkg}$ the total signal measured by the detector. We will divide the energy range between 4 and 30 keV in $n = 7$ equidistant energy bins. For the discrimination between the signal and the background we calculate the variance χ^2:

$$\chi^2 = \sum_{i=1}^{n} \left(\frac{N_i^{tot} - N_i^{bkg}}{\sigma_i} \right)^2 \ . \tag{2.5}$$

Here we are assuming a Gaussian error $\sigma_i = \sqrt{\frac{N_i^{tot}}{M \cdot T}}$ on the measurement, where M is the detector mass and T the exposure time.

We show in Fig.1 an example of a signal with a standard neutron background in a XENON–like (100 kg) experiment, after 3 years of data acquisition, as a function of the recoil energy. For a WIMP mass of 100 GeV and a WIMP–nucleon cross-section of 10^{-9} pb, such an experiment would reach a pretty large χ^2 per degree of freedom ($\chi^2_{\rm red}$) , of the order of 60.

2.2 The XENON experiment

The XENON experiment at the Gran Sasso national laboratory aims at the direct detection of dark matter via its elastic scattering off xenon nuclei. It was deployed underground in March 2006 and has been in continuous operation for a period of about one year. It allows the simultaneous measurement of direct scintillation in the liquid and of ionization, via proportional scintillation in the gas. In this way, XENON discriminates signal from background for a nuclear recoil energy as small as 4.5 keV. Currently a 10 kg detector is being used, but the final mass will be 1 ton of liquid xenon. In Fig.2, we show the sensitivity curve for *Xenon10* ($M = 10$ kg) and *Xenon1T* ($M = 1$ ton) for $T = 3$ years of data acquisition.

In our study, following Ref. [9] we will consider 7 energy bins between 4 and 30 keV and 3 years of data acquisition for a 100 kg XENON experiment. Such experimental conditions and time of exposure can be achieved after the 6 years of GLAST mission and justify the comparison between the two detection modes. We could take into account non-zero background using simulations of the recoil spectra of neutrons in our analysis, and this would significantly degrade the sensitivity of the detector. However, this would involve a much more detailed study of the detector components (shielding, etc.), and we will not carry it out. In that sense, our results will be the most optimistic.

3 Indirect detection

3.1 Differential event rate

The spectrum of gamma–rays generated in dark matter annihilations and coming from a direction forming an angle ψ with respect to the galactic center is

$$\Phi_\gamma(E_\gamma, \psi) = \sum_i \frac{dN_\gamma^i}{dE_\gamma} Br_i \langle \sigma v \rangle \frac{1}{8\pi m_\chi^2} \int_{line\ of\ sight} \rho^2 \ dl \ , \tag{3.6}$$

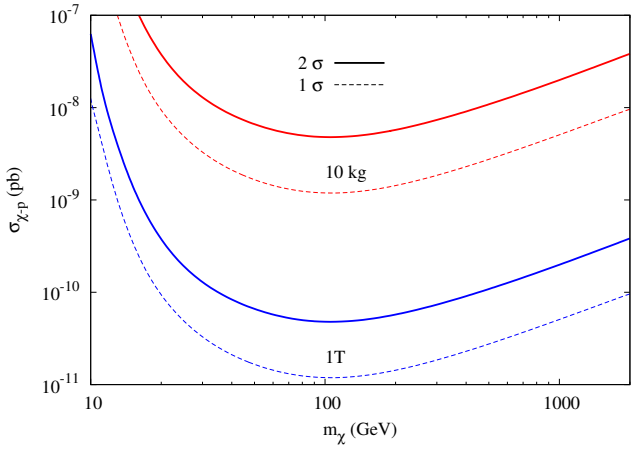

Figure 2: Spin-independent WIMP-nucleon cross-section versus WIMP mass for $\chi^2 = 1, 4$ and M=10 kg and 1 ton.

	a (kpc)	α	β	γ	$\bar{J}(4 \cdot 10^{-3}\mathrm{sr})$
NFW	20	1	3	1	$5.859 \cdot 10^2$
$\mathrm{NFW_c}$	20	0.8	2.7	1.45	$3.254 \cdot 10^4$
Moore et al.	28	1.5	3	1.5	$2.574 \cdot 10^4$
$\mathrm{Moore_c}$	28	0.8	2.7	1.65	$3.075 \cdot 10^5$

Table 1: NFW and Moore et al. density profiles without and with adiabatic compression ($\mathrm{NFW_c}$ and $\mathrm{Moore_c}$ respectively) with the corresponding parameters, and values of $\bar{J}(\Delta\Omega)$.

where the discrete sum is over all dark matter annihilation channels, dN_γ^i/dE_γ is the differential gamma–ray yield, $\langle\sigma v\rangle$ is the annihilation cross-section averaged over its velocity distribution, Br_i is the branching ratio of annihilation into "i" final state, and ρ is the dark matter density. We describe in more detail the method followed, in order to obtain the spectral function describing the standard model particle decay into γ-rays, in the Appendix.

It is customary to rewrite Eq. (3.6) introducing the dimensionless quantity J (which depends only on the dark matter distribution):

$$J(\psi) = \frac{1}{8.5 \text{ kpc}} \left(\frac{1}{0.3 \text{ GeV/cm}^3} \right)^2 \int_{line\ of\ sight} \rho^2(r(l,\psi))\ dl\ . \tag{3.7}$$

After having averaged over a solid angle, $\Delta\Omega$, the gamma–ray flux can now be expressed as

$$\begin{aligned} \Phi_\gamma(E_\gamma) &= 0.94 \cdot 10^{-13}\ \mathrm{cm^{-2}\ s^{-1}\ GeV^{-1}\ sr^{-1}} \\ &\cdot \sum_i \frac{dN_\gamma^i}{dE_\gamma} \left(\frac{Br_i \langle\sigma v\rangle}{10^{-29}\mathrm{cm^3 s^{-1}}} \right) \left(\frac{100 \text{ GeV}}{m_\chi} \right)^2 \overline{J}(\Delta\Omega)\Delta\Omega\ . \end{aligned} \tag{3.8}$$

The value of $\overline{J}(\Delta\Omega)\Delta\Omega$ depends crucially on the dark matter distribution. The most common parametrization of the different profiles that have been proposed in the literature is

$$\rho(r) = \frac{\rho_0[1+(R_0/a)^\alpha]^{(\beta-\gamma)/\alpha}}{(r/R_0)^\gamma[1+(r/a)^\alpha]^{(\beta-\gamma)/\alpha}} \ , \tag{3.9}$$

where ρ_0 is the local (solar neighborhood) halo density, a is a characteristic length, and R_0 the distance from the Sun to the galactic center. As mentioned above, we will use $\rho_0 = 0.3$ GeV/cm^3 throughout the paper, but since this is just a scaling factor in the analysis, modifications to its value can be straightforwardly taken into account in the results. N–body simulations suggest a cuspy inner region of dark matter halo with a distribution where γ generally lies in the range 1 (NFW profile [11]) to 1.5 (Moore et al. profile [12]), producing a profile with a behavior $\rho(r) \propto r^{-\gamma}$ at small distances. Over a solid angle of $4 \cdot 10^{-3}$ sr, such profiles can lead from $\overline{J}(\Delta\Omega) \sim 5.859 \cdot 10^2$ to $2.574 \cdot 10^4$. Moreover, if we take into account the baryon distribution in the Galaxy, we can predict even more cuspy profiles with γ in the range 1.45 to 1.65 ($\overline{J}(\Delta\Omega) \sim 3.254 \cdot 10^4 - 3.075 \cdot 10^5$) through the adiabatic compression process (see the study of Refs. [13, 14]). We summarize the parameters used in our study and the values of $\bar{J}$ for each profile in Table 1. It is worth noticing here that we are neglecting the effect of clumpyness, even though other studies showed that, depending upon assumptions on the clumps' distribution, in principle an enhancement of a factor 2 to 10 is possible [15]. In this respect, the following predictions on the gamma-ray flux from the galactic center are conservative.

3.2 Modeling the galactic center background.

HESS [16] has measured the gamma–ray spectrum from the galactic center in the range of energy $\sim$ [160 GeV–10 TeV]. The collaboration claims that the data are fitted by a power–law

$$\phi_{\rm bkg}^{\rm HESS}(E) = F_0 \ E_{\rm TeV}^{-\alpha}, \tag{3.10}$$

with a spectral index $\alpha = 2.21 \pm 0.09$ and $F_0 = (2.50 \pm 0.21) \cdot 10^{-8}$ m^{-2} s^{-1} TeV^{-1}. The data were taken during the second phase of measurements (July–August, 2003) with a χ^2 of 0.6 per degree of freedom. Because of the constant slope power–law observed by HESS, it turns out possible but difficult to conciliate such a spectrum with a signal from dark matter annihilation [14, 17]. Indeed, final particles (quarks, leptons or gauge bosons) produced through annihilations give rise to a spectrum with a continuously changing slope. Several astrophysical models have been proposed in order to match the HESS data [18]. In the present study we consider the astrophysical background for gamma–ray detection as the one extrapolated from the HESS data with a continuous power–law over the energy range of interest (≈ 1 – 300 GeV). As was recently underlined in Ref. [19], GLAST sensitivity will be affected by the presence of such an astrophysical source. Note that the WIMP masses that we shall obtain in our parameter space $\lesssim 1$ TeV avoid any conflict with the observations of HESS.

In addition, we have also taken into account the EGRET data [20] in our background at energies below 10 GeV ($\phi_{\rm bkg}^{\rm EGRET}(E)$), as they can affect the sensitivity of the analysis. Indeed, the extrapolation of the gamma–ray fluxes measured by HESS down to energies as low as 1 GeV is likely to be an underestimation of the gamma–ray background in the galactic center, as EGRET measurements are one to two orders of magnitude higher than the HESS extrapolation. We thus decided to take as background an interpolation between the HESS extrapolation and the EGRET data below 10 GeV to stay as conservative as possible in evaluating the gamma–ray background.

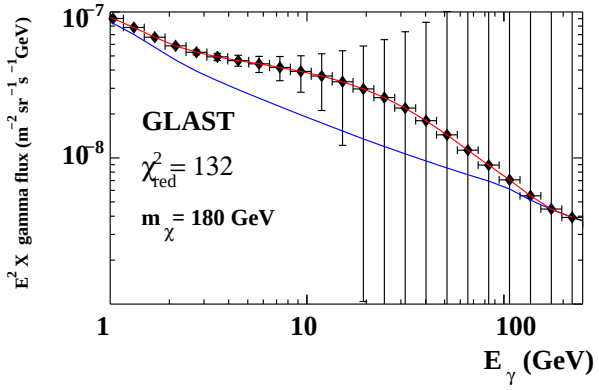

Figure 3: GLAST expectations for gamma–ray fluxes in the case of a WIMP mass $m_\chi = 180$ GeV and cross section $\langle \sigma v \rangle = 3 \cdot 10^{-26}$ cm^{3}s^{-1}. A NFW halo profile has been adopted. The error bars shown are those projected for the GLAST experiment after a six-year mission run, assuming the galactic center will be within its field–of–view 50% of the time. The lower (blue) line is the background–only prediction. The χ^2_{red} is 132, giving a signal clearly distinguishable from the background.

Finally, we will consider the diffuse background of gamma rays in the region surrounding the galactic center. We will describe the spectrum of the background using the HESS observation from the Galactic Center Ridge [16], which can be described by

$$\phi^{\rm diff}_{\rm bkg}(E) = 1.1 \cdot 10^{-4} E^{-2.29}_{\rm GeV} {\rm GeV}^{-1}{\rm cm}^{-2}{\rm s}^{-1}{\rm sr}^{-1} \ . \tag{3.11}$$

We will consider in our analysis the inner $2^o \times 2^o$ field of view ($\Delta\Omega = 4 \cdot 10^{-3}$ sr) with 50 energy bins logarithmically distributed between 1 and 300 GeV. During the completion of our work, the authors of Ref. [8] gave a more detailed and sophisticated statistical analysis of the diffuse background, adopting an overall normalization around the galactic center and taking into account a statistical spread function as GLAST would be able to probe in this region. However, we have checked that our results are not significantly modified and we recover similar results concerning the prospects of GLAST.

3.3 The GLAST experiment

The space–based gamma–ray telescope GLAST [10] is scheduled for launch in May 2008 for a five-year mission. It will perform an all-sky survey covering a large energy range (≈ 1 – 300 GeV). With an effective area and angular resolution on the order of 10^4 cm^2 and 0.1^o ($\Delta\Omega \sim 10^{-5}$ sr) respectively, GLAST will be able to point and analyze the inner center of the Milky Way (~ 7 pc). Concerning the requested condition on the χ^2 for a signal discovery, we have used an analysis similar to the one considered in the case of direct detection in section 2.1, with a six-year mission run, assuming the galactic center will be within its field–of–view 50% of the time [10, 21]. In Fig. 3 we show the ability of GLAST to identify a signal from dark matter annihilation for a WIMP mass of 180 GeV. The error bars shown are projected assuming Gaussian statistic, and we adopt the background described above including Poisson noise. In the following, we will concentrate on a process which gives 100% annihilation to WW. We have checked that the dependence on the final state does not influence significantly the general results of the study, except in the case of leptonic final states. This will be studied

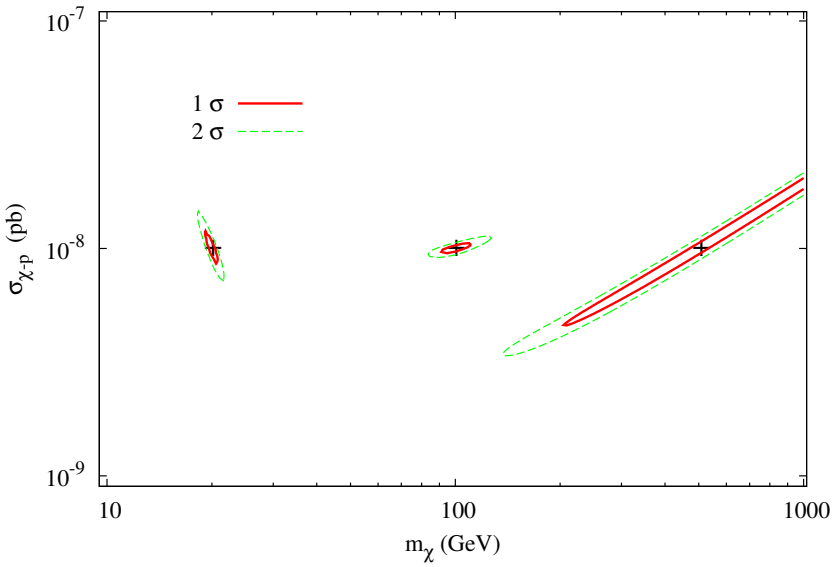

Figure 4: Distribution of the maximum likelihood WIMP mass, m_χ, and cross-section, $\sigma_{\chi-p}$, for 3 years of exposure in a 100 kg XENON experiment, for $m_\chi = 20,\ 100,\ 500$ GeV and $\sigma_{\chi-p} = 10^{-8}$ pb. The inner (full) and outer (dashed) lines represent the 1 and 2σ region respectively. The crosses denote the theoretical input parameters ($\sigma_{\chi-p}$, m_χ).

in a specific case in Section 5 dedicated to the ILC experiment.

4 Direct versus indirect detection experiments

We show in Fig. 4 (Fig. 5) the ability of XENON (GLAST) to determine the mass and scattering (annihilation) cross-section for a 20 (50), 100 and 500 GeV WIMP. We clearly see how sensitive both experiments are to light WIMPs: the precision can easily reach the percent level for XENON and GLAST for[1] $m_\chi \lesssim 50$ GeV. Indeed, the recoil energy of the nucleus depends on the reduced mass (see Eq. 2.1). For WIMPs much heavier than the nucleus mass (~ 100 GeV for Xenon), $m_r \sim m_N$, and therefore independent of the WIMP mass. This is clearly reflected in the uncertainties at 1 and 2σ in Fig. 4 for a 500 GeV WIMP. On the other hand, the gamma–ray spectrum will give more precise measurements if the mass of the WIMP lies within the GLAST sensitivity range. Indeed, the shape of the spectrum will be easily reconstructed above the HESS/EGRET and diffuse background if the endpoint of the annihilation spectrum lies within the energy range reachable by GLAST $[0.1 - 300$ GeV]. Furthermore, we have studied the influence of the variation of the inner slope of the halo profile on the resolution of the WIMP mass. In addition to the NFW profile, we have considered some NFW–like profiles, allowing the γ parameter in Eq. (3.9) to vary from its original value by 10%. This is shown in Fig. 6, where in addition to the NFW halo profile ($\gamma = 1$) we also study profiles with $\gamma = 0.9, 1.1$. As expected, the larger the γ is, the more enhanced the galactic gamma ray flux becomes, and the better the WIMP mass resolution turns out

[1] During the finalization of this work, Drees and Shan in Ref. [7] showed that one can even increase such a precision with a combined analysis of two experiments of direct detection.

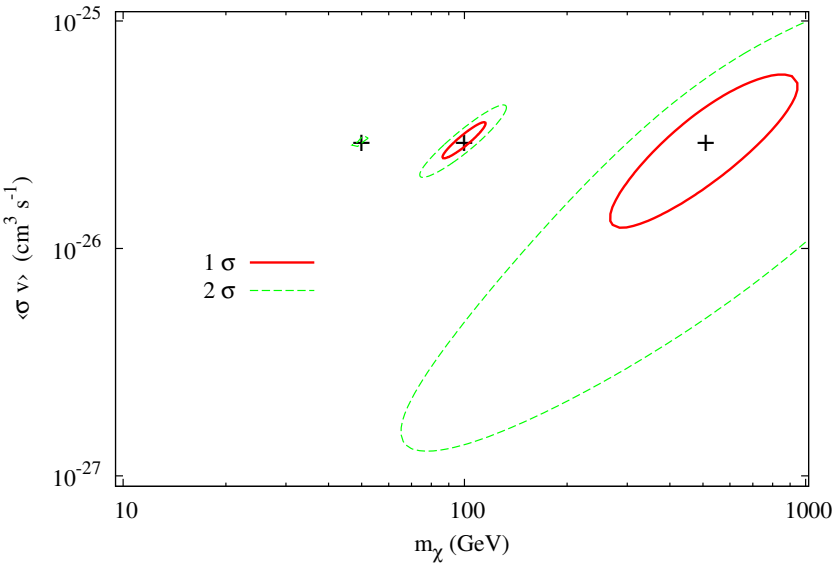

Figure 5: Distribution of the maximum likelihood WIMP mass, m_χ, and annihilation cross-section, $\langle\sigma v\rangle$, after 6 years of observation (50% of time exposure) of the galactic center with GLAST, with the hypothesis of a NFW halo profile, for $m_\chi = 50,\ 100,\ 500$ GeV and $\langle\sigma v\rangle = 3 \cdot 10^{-26}$ cm^{3}s^{-1}. The inner (full) and outer (dashed) lines represent the 1 and 2σ region respectively. The crosses denote the theoretical input parameters ($\langle\sigma v\rangle$, m_χ).

to be. It is worth noticing here that in the case of a compressed NFW profile ($\gamma \sim 1.45$), the precision of GLAST increases by two orders of magnitude. Finally, let us remark from Figs. 4 and 5, how two completely different means of observation, with completely different signal/background physics, are in fact competitive (and so complementary) in the search for the dark matter.

In Fig. 7 we compare the precision level for both experiments as a function of the WIMP mass, for different values of the spin-independent cross-section (10^{-7}, 10^{-8} and 10^{-9} pb) and for different halo profiles. We see that at 95% of confidence level GLAST, after 3 years of exposure (6 years of taking data at 50% of time exposure), will have an equivalent sensitivity to a 100 kg XENON-like experiment after 3 years of running if $\sigma_{\chi-p} \lesssim 5 \cdot 10^{-9}$ pb, *independently on the WIMP mass*. The indirect detection by GLAST will always be able to give an upper bound on the WIMP mass for $m_\chi \sim 100$ GeV, whereas a XENON-like 100 kg experiment would only give a lower bound value if $\sigma_{\chi-p} \lesssim 10^{-9}$ pb. In all cases, the lower bounds given by GLAST for a NFW halo profile are similar to the ones given by a XENON-like 100 kg experiment for any WIMP mass if $\sigma_{\chi-p} \lesssim 10^{-9}$ pb.

To compare the uncertainties on the WIMP mass expected from direct and indirect detection modes, we plotted in Fig. 8 $\frac{\Delta m_\chi}{m_\chi}$ as a function of the WIMP mass for different values of $\sigma_{\chi-p}$ and different types of halo profiles, NFW and NFW$_c$. One can clearly see in the left panel of Fig. 8 that GLAST will be competitive with XENON 100 kg to measure the WIMP mass in the case of a NFW halo profile only if $\sigma_{\chi-p} \lesssim 10^{-8}$ pb. For a NFW compressed halo profile (right panel of Fig. 8), the precision obtained by GLAST is much better. The experiment would even be able to measure the WIMP mass at the 10% level for a 1 TeV dark matter candidate, something which will be unreachable by any near–future direct detection project.

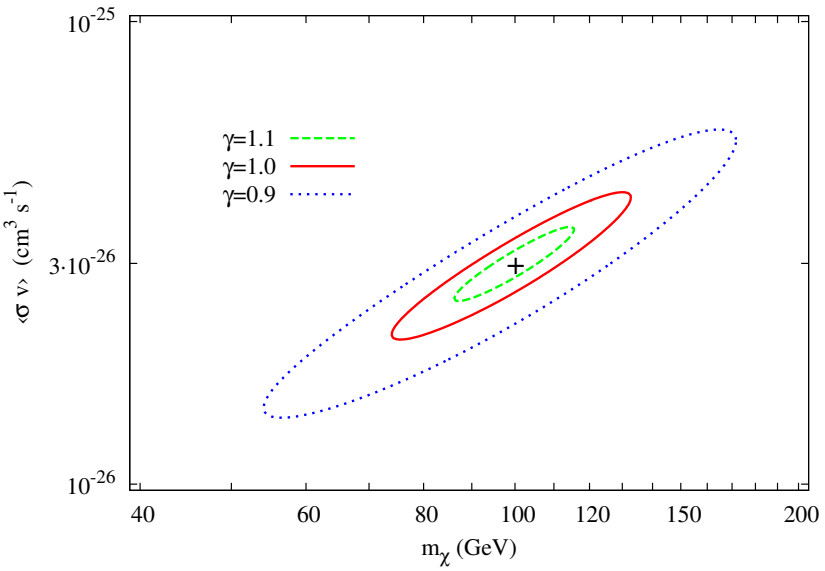

Figure 6: NFW–like halo profile with $\gamma = 0.9$, 1 (NFW) and 1.1 at 95% confidence level.

5 WIMP dark matter at present and future colliders

Among the most important sources of information concerning WIMP dark matter are, obviously, collider experiments, both present, such as the Tevatron or the oncoming Large Hadron Collider (LHC) and future, such as the International Linear Collider (ILC). In fact, there is a quite general agreement on the fact that despite the significant progress in astroparticle physics experiments, which manage to impose more and more constraints on various models, collider experiments remain an irreplaceable source of information for particle physics. It is quite natural thus, to examine the potential of colliders to constrain WIMP properties. We will examine the extent at which astroparticle and collider experiments become competitive, trying at the same time to stay as model-independent as possible.

This last point is, in fact, the major difficulty in treating collider experiments to extract astroparticle data: most studies performed for new physics at colliders are very strongly model dependent. This is almost unavoidable for the case of the LHC, due to the hadronic nature of the colliding particles. The large uncertainties on the parton distribution functions (and, hence, on the initial energy of the colliding particles/partons) render it extremely difficult (in fact, practically impossible) to look beyond the transverse plane. This fact obviously limits -up to a certain point- the precision that could be obtained with respect to, for example, an e^+e^- collider. As a result, it is quite difficult to make predictions in a model-independent way, since a whole set of parameters must be taken into account in order to perform concrete predictions. The cruciallity of these uncertainties will become clearer in the following.

5.1 The Approach

Recently, an approach was proposed in references [22, 23] which allows to actually perform a model-independent study of WIMP properties at lepton colliders (such as the ILC project). The goal we pursue is to extract constraints which are as stringent as possible for a generic

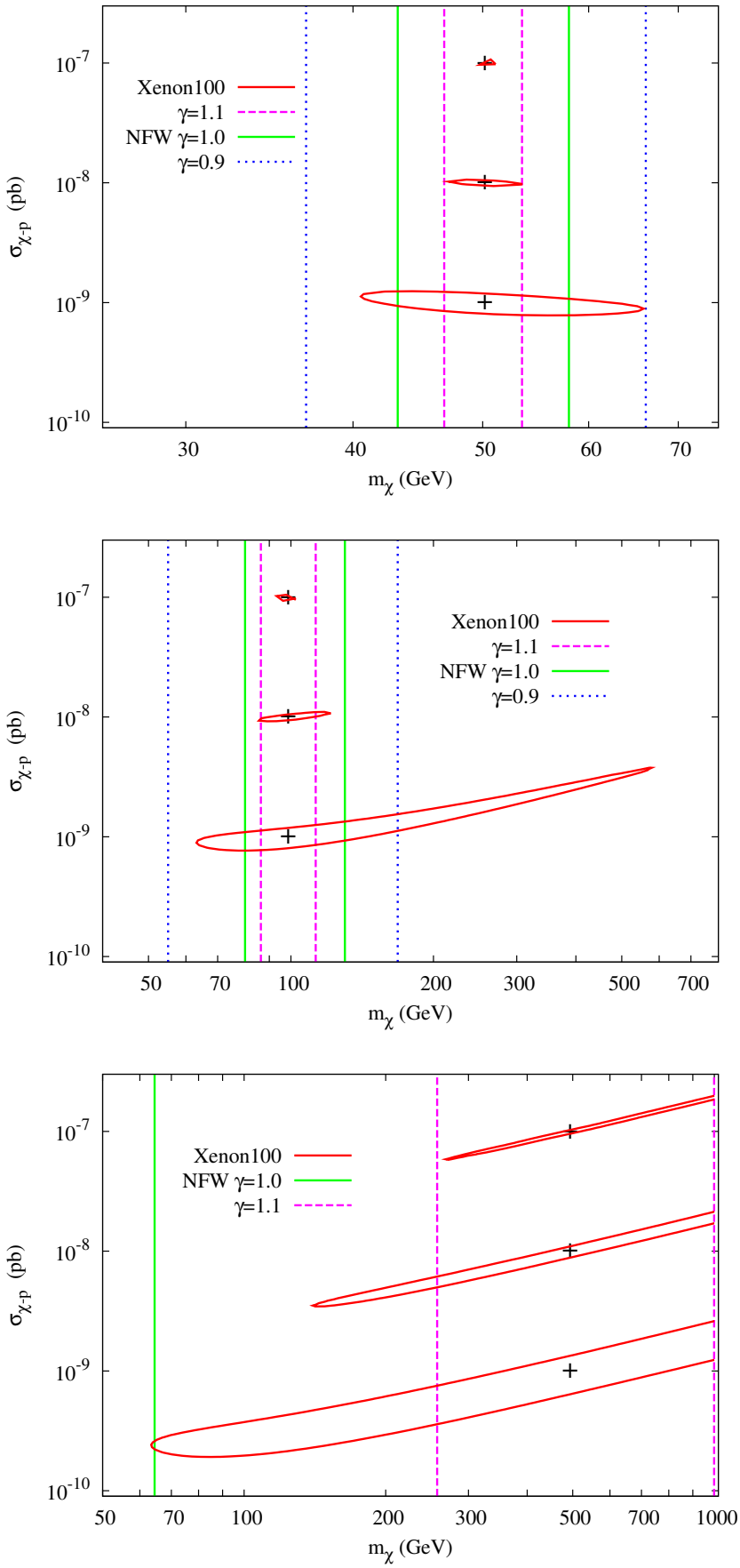

Figure 7: Comparison between 100 kg XENON-like experiment and GLAST sensitivity in the case of different halo profiles, at 95% of confidence level, for several WIMP masses (50, 100 and 500 GeV) and WIMP–nucleon cross-sections (10^{-7}, 10^{-8} and 10^{-9} pb). In each panel the cross denotes the input parameters.

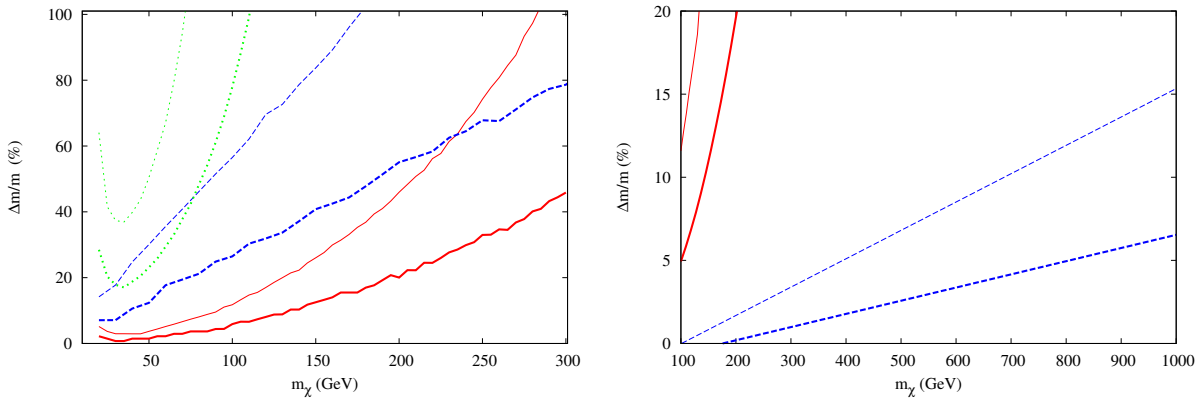

Figure 8: 1 and 2σ error for GLAST experiment (blue-dashed) for $\langle\sigma v\rangle = 3\cdot 10^{-26}$ cm^{3}s^{-1} in the case of a NFW (left) and NFW$_c$ (right) halo profile, compared with the XENON 100 kg experiment for $\sigma_{\chi-p} = 10^{-7}$ pb (red-solid) and $\sigma_{\chi-p} = 10^{-9}$ pb (green-dotted).

dark matter candidate. A generic WIMP can annihilate into pairs of standard model particles:

$$\chi + \chi \longrightarrow X_i + \bar{X}_i \ . \tag{5.12}$$

However, the procedure taking place in a collider is the opposite one, having only one species of particles in the initial state. The idea proposed in Ref. [22] is to correlate the two processes in some way. This can be done through the so-called "detailed balancing" equation, which reads:

$$\frac{\sigma(\chi+\chi\to X_i+\bar{X}_i)}{\sigma(X_i+\bar{X}_i\to\chi+\chi)} = 2\frac{v_X^2(2S_X+1)^2}{v_\chi^2(2S_\chi+1)^2} \ , \tag{5.13}$$

where v_i and S_i are respectively the velocity and the spin of the particle i. The cross-section $\sigma(\chi\chi\to X_i\bar{X}_i)$ is only averaged over spins.

The total thermally averaged WIMP annihilation cross-section can be expanded as

$$\sigma_i v = \sum_{J=0}^{\infty} \sigma_i^{(J)} v^{2J} \ , \tag{5.14}$$

where J is the angular momentum of each annihilation wave. Now, for low velocities, the lowest-order non-vanishing term in the last equation will be dominant. So, we can express the total annihilation cross-section as a sum of the partial ones over all possible final states for the dominant partial wave J_0 in each final state:

$$\sigma_{an} = \sum_i \sigma_i^{(J_0)} \ . \tag{5.15}$$

Next, we can define the "annihilation fraction" κ_i into the standard model particle pair $X_i - \bar{X}_i$:

$$\kappa_i = \frac{\sigma_i^{(J_0)}}{\sigma_{an}} \ . \tag{5.16}$$

By combining Eqs. (5.13) and (5.16) we can obtain the following expression for the WIMP pair-production cross-section:

$$\sigma(X_i\bar{X}_i\to 2\chi) = 2^{2(J_0-1)}\kappa_i\sigma_{an}\frac{(2S_\chi+1)^2}{(2S_X+1)^2}\left(1-\frac{4M_\chi^2}{s}\right)^{1/2+J_0} \ . \tag{5.17}$$

Now, a few remarks should be made about the validity of this formula:

- Equation (5.17) is valid for WIMP pair-production taking place at center-of-mass energies just above the pair-production threshold.
- The detailed balancing equation is valid if and only if the process under consideration is characterized by time-reversal and parity invariance. It is well known that weak interactions violate both of them, up to some degree, which we ignore in this treatment.

A process of the form $X_i\bar{X}_i \longrightarrow \chi\chi$ is not visible in a collider, since WIMPs only manifest themselves as missing energy. At least one detectable particle is required for the event to pass the triggers. An additional photon from initial state radiation (ISR) is required to be recorded on tape: $X_i\bar{X}_i \longrightarrow \chi\chi\gamma$. We can correlate the WIMP pair-production process to the radiative WIMP pair-production for photons which are either soft or collinear with respect to the colliding beams. In this case, the two processes are related through [22] :

$$\frac{d\sigma(e^+e^- \to 2\chi + \gamma)}{dx\, d\cos\theta} \approx \mathcal{F}(x, \cos\theta)\tilde{\sigma}(e^+e^- \to 2\chi) \ , \tag{5.18}$$

where $x = 2E_\gamma/\sqrt{s}$, θ is the angle between the photon direction and the direction of the incoming electron beam, $\tilde{\sigma}$ is the WIMP pair-production cross-section produced at the reduced center of mass energy $\tilde{s} = (1-x)s$, and $\mathcal{F}$ is defined as:

$$\mathcal{F}(x, \cos\theta) = \frac{\alpha}{\pi}\frac{1+(1-x)^2}{x}\frac{1}{\sin^2\theta} \ . \tag{5.19}$$

Now, by combining Eqs. (5.18) and (5.17) we get the master equation:

$$\frac{d\sigma}{dx\, d\cos\theta}(e^+e^- \to 2\chi+\gamma) \approx \frac{\alpha\kappa_e\sigma_{an}}{16\pi}\frac{1+(1-x)^2}{x}\frac{1}{\sin^2\theta}2^{2J_0}(2S_\chi+1)^2\left(1-\frac{4M_\chi^2}{(1-x)s}\right)^{1/2+J_0} \ . \tag{5.20}$$

The problem is that very collinear photons fall outside the reach of any detector, due to practical limitations in the coverage of the volume around the beam pipe. Also, typically, lower cuts are included in the detected transverse momentum of photons, $p_T = E_\gamma \sin\theta$, in order to avoid excessive background signals at low energies. So, if we are to use this approach, we have to examine its validity outside the soft/collinear region. The accuracy of the collinear approximation for hard photons at all angles has been discussed in the original paper [22], with the conclusion that the approach works quite well.

However, an important point should be taken into account here. From the previous discussion on the validity of the method, we have to impose specific kinematical cuts on the detected photons. We consider the following conditions:

- We demand an overall condition $\sin\theta \geq 0.1$ and $p_T \geq 7.5$ GeV in order to assure the detectability of the photons.
- In order to assure the fact that any photon under examination corresponds to non-relativistic WIMPs, we demand $v_\chi^2 \leq 1/2$. This gives a lower kinematical cut, along with an upper cut corresponding just to the endpoint of the photon spectrum:

$$\frac{\sqrt{s}}{2}\left(1-\frac{8M_\chi^2}{s}\right) \leq E_\gamma \leq \frac{\sqrt{s}}{2}\left(1-\frac{4M_\chi^2}{s}\right) \ . \tag{5.21}$$

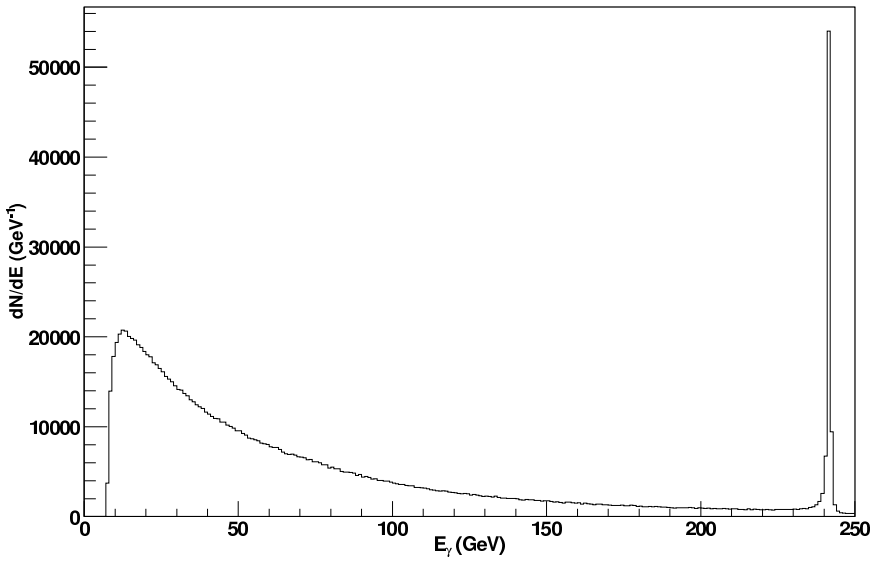

Figure 9: Radiative neutrino production background $e^+e^- \to \nu\bar{\nu}\gamma$ for the ILC, for an unpolarized initial state.

These conditions present a flaw: the energy limits depend on the mass we wish to constrain. On the other hand, for the reasons explained before, we cannot treat the signals without imposing such kinds of cuts, if we do not want either to abuse the method or stick to heavy WIMPs (which, for kinematical reasons, cannot be relativistic). The only way to evade this problem is to suppose that other dark matter detection experiments (or, eventually, the LHC in the framework of specific models) will have already provided us with some sort of limits on the WIMP mass. In this case, having an idea of the region in which the WIMP mass falls, we can also estimate the cuts that will safely keep us outside the relativistic region and only consider photons within this region.

The main source of background events is the standard model radiative neutrino production, $e^+e^- \longrightarrow \nu\bar{\nu}\gamma$. Apart from these background events, various models predict additional signals of the form "γ + missing energy", one of the most well-known examples being radiative sneutrino production [24, 25], predicted in the framework of several supersymmetric models. In the spirit of staying as model-independent as possible, we will ignore all possible beyond standard model processes.

5.2 Basic Results

5.2.1 Non-polarized beams

We place ourselves in the framework of the ILC project with a center-of-mass energy of $\sqrt{s} = 500$ GeV and an integrated luminosity of 500 fb^{-1}. In order to estimate the background events, we used the CalcHEP code [26, 27] to generate 1.242.500 $e^+e^- \longrightarrow \nu\bar{\nu}\gamma$ events, corresponding to the aforementioned conditions. The total radiative neutrino production background can be seen in Fig. 9. The peak at $E_\gamma = \sqrt{s}/2 \cdot (1 - M_Z^2/s) \simeq 241.7$ GeV corresponds to the radiative returns to the Z resonance.

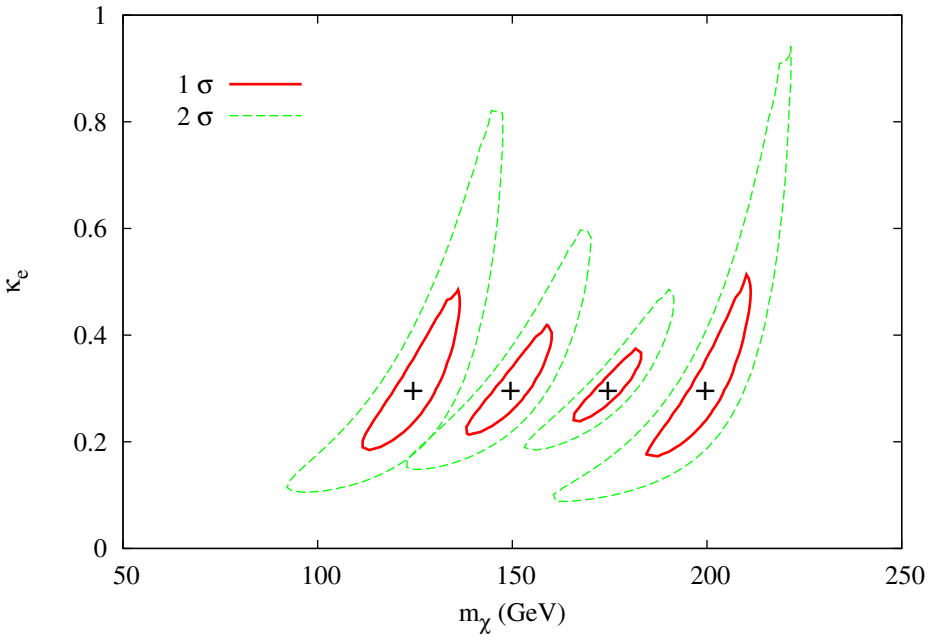

Figure 10: Distribution of the maximum likelihood WIMP mass and annihilation fraction for the ILC in the (m_χ, κ_e) plane, for $\kappa_e = 0.3$ and $m_\chi = 125, 150, 175$ and 200 GeV. The inner (full lines) and outer (dashed lines) represent the 1 and 2σ region respectively.

We use the same χ^2 method as previously. We generate a predicted "observable" spectrum for given values of the WIMP mass and the annihilation fraction. During this study, we do not proceed to a (more realistic) full detector simulation, as done for example in Ref. [28], but stick to prediction levels in order to perform as thorough a scan as possible in the (m_χ, κ_e) parameter space and to have a picture of the "a priori" potential of the method.

Figure 10 shows the predicted ability of the ILC to determine WIMP masses and annihilation fractions for four points in the (m_χ, κ_e) parameter space for a 1σ and 2σ precision. These results concern WIMPs with spin $S_\chi = 1/2$ and an angular momentum $J_0 = 1$ which corresponds to an annihilation cross-section $\sigma_{an} = 7$ pb [22]. As can be seen, we are able to constrain quite significantly the WIMP mass ($20\% - 40\%$ precision), while constraints on κ_e are weaker.

Figure 11 shows the relative error $(\Delta m_\chi / m_\chi)$ for the mass reconstruction as a function of m_χ, for $\kappa_e = 0.3$ and a 2σ confidence level. The solid line corresponds to the proper treatment including kinematical cuts. For indicative reasons, we also show the abused results obtained if we do not impose kinematical cuts on the photon energy (dashed line). The amelioration of the method's efficiency is obvious, although this is after all a false fact, since we include regions in which the approach is not valid. Above $m_\chi \simeq 175$ GeV the two lines become identical, since the WIMPs cannot be relativistic. The capacity of the method peaks significantly for masses of the order of 175 GeV because around this value we reach an optimal combination of phase space volume and available spectrum that passes the kinematical cuts and can, hence, be used for the calculation of the relevant χ^2; whereas as we move away from this value the accuracy tends to fall.

Let us make a final remark on the possibility of adopting a similar approach in the case

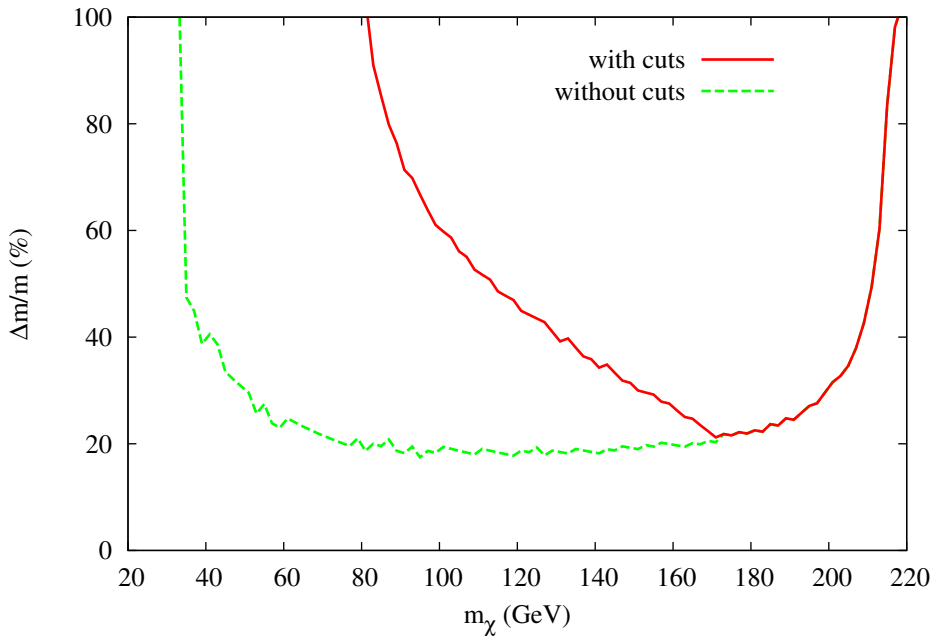

Figure 11: Relative error in a generic WIMP mass determination, for $\kappa_e = 0.3$ and at a 2σ confidence level. The solid line corresponds to the results obtained after imposing the proper kinematical cuts, whereas the dashed line to the case where we do not take these limits in consideration.

of the LHC. As we argued before, the large uncertainties entering the parton distribution functions and, hence, the large uncertainty in the collision energy, affect significantly the precision of the whole procedure (which is, already, based on approximations). Formally, in order to perform such a study for the LHC, the computed cross-sections must be convoluted with the proton form factors. As an additional element, the photon background in the LHC is expected to be much greater than in the ILC. The possibility of determining WIMP properties through a model-independent method at the LHC has been addressed to in Ref. [29], where the authors conclude that WIMP detection will be extremely difficult, if even possible.

5.2.2 Polarized beams

The reach of the ILC can be further increased by polarizing the beams. For polarized beams, the signal cannot be fully characterized by κ_e; instead, four independent annihilation fractions are needed, corresponding to the four possible e^+e^- helicity configurations.

To apply Eq. (5.20) to this case, we make the replacement:

$$\begin{aligned} \kappa_e \;\; \to \;\; & \frac{1}{4}(1+P_-)\,\left[(1+P_+)\,\kappa(e^R_- e^L_+) + (1-P_+)\,\kappa(e^R_- e^R_+)\right] \\ + \;\; & \frac{1}{4}(1-P_-)\,\left[(1+P_+)\,\kappa(e^L_- e^L_+) + (1-P_+)\,\kappa(e^L_- e^R_+)\right] \;\; , \end{aligned} \tag{5.22}$$

where $P_\pm$ are the polarizations of the positron and the electron beams. As in ref [22, 28], let us assume that the WIMP couplings to electrons conserve both helicity and parity: $\kappa(e^R_- e^L_+) = \kappa(e^L_- e^R_+) = 2\,\kappa_e$ and $\kappa(e^R_- e^R_+) = \kappa(e^L_- e^L_+) = 0$.

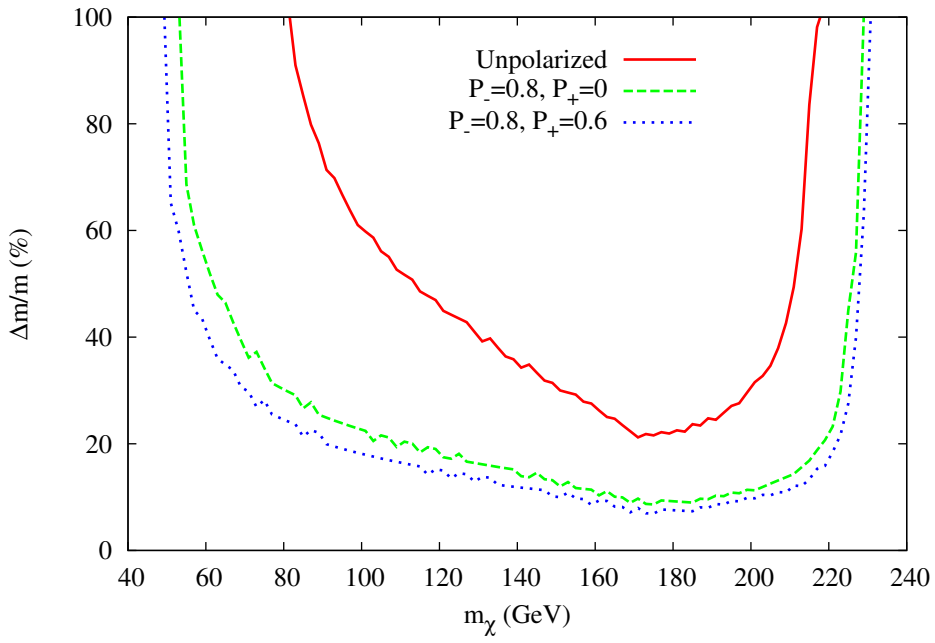

Figure 12: Relative error in a generic WIMP mass determination, for three cases of beam polarization, including all proper kinematical cuts.

m_χ	XENON	GLAST	ILC
50 GeV	± 1 GeV	± 8 GeV	–
100 GeV	$\pm$ 6 GeV	$-25/+32$ GeV	$-40/+20$ GeV
175 GeV	$-25/+35$ GeV	$-70/+100$ GeV	$-20/+15$ GeV
500 GeV	–	–	–

Table 2: Precision on a WIMP mass expected from the different experiments at 2σ after 3 years of exposure, $\sigma_{\chi-p} = 10^{-7}$ pb a NFW profile and a 500 GeV linear collider unpolarized with a luminosity of $500 fb^{-1}$

In Fig.12 we show the relative error for the mass reconstruction for $\kappa_e = 0.3$ and 2σ confidence level, for the unpolarized scenario and for two different polarizations: $(P_-, P_+) = (0.8, 0)$ and $(0.8, 0.6)$.

6 Complementarity

In Fig.13 we compare the precision levels for direct and indirect detection experiments, along with the corresponding results of the method we followed for the ILC for two cases of WIMPs masses, $m_\chi = 100$ GeV and 175 GeV, and $\kappa_e = 0.3$. We plot the results in the (m_χ, κ_e) plane. This is done as the κ_e parameter entering the ILC treatment presented before is, in fact, the same parameter as the corresponding branching ratio $Br_i = \frac{\langle \sigma_i v \rangle}{\langle \sigma v \rangle}$ appearing in eq. (3.6) for $i = e$.

The blue-dotted line corresponds to a 100 kg XENON-like experiment, where the WIMP-nucleus cross-section has been assumed to be 10^{-7} pb. The green-dashed line depicts the results for a GLAST-like experiment assuming a NFW halo profile. The total annihilation cross-section into standard model particles has been taken to be $\langle \sigma v \rangle = 3 \cdot 10^{-26}$ cm^{3}s^{-1}. The red-plain line represents our results for an ILC-like collider, with non-polarized beams. All the results are plotted for a 2σ precision level.

We can see that for different regions of the WIMP mass, the three kinds of experiments that we have used as prototypes can act in a highly complementary way. For example, for the case of a 100 GeV WIMP, indirect detection or an ILC-like experiment alone can provide us with limited precision both for the WIMP mass (of the order of 60%) and the κ_e parameter (where the results are even worse). Combined measurements can dramatically increase the precision, reaching an accuracy of 25% in mass. If we additionally include direct detection measurement, we reach a precision of the order of 9%.

For the case of a 175 GeV WIMP, a point where the unpolarized ILC sensitivity peaks, we see that the dominant information comes from this source. Nevertheless, even if we only combine direct and indirect detection experiments, we see that we can, in fact, acquire non-negligible constraints on the dark matter candidate mass.

To summarize the analysis, we show in Table 2 the precision expected for several interesting dark matter masses. Whereas a light WIMP (50 GeV) can be reached by both types of dark matter experiments with a relatively high level of precision, our analysis fails in the ILC case because of the relativistic nature of the WIMP. On the contrary, the ILC would be particularly efficient to discover and measure a WIMP with a mass of about 175 GeV. Concerning a 500 GeV WIMP, which is kinematically unreachable at the linear collider, it would be difficult to be observed by GLAST or XENON. Only a lower bound (250 GeV for XENON, 150 GeV for GLAST) could be determined experimentally.

7 Conclusions

A Weakly Interacting Massive Particle (WIMP), with mass lying from the GeV to the TeV scale, is one of the preferred candidates for the dark matter of the Universe.

We have discussed the possibility of identifying WIMP properties in a model-independent way. For that we have considered direct and indirect searches, and in particular the interesting cases of a XENON-like 100 kg. experiment and the GLAST satellite. We have shown that whereas direct detection experiments will probe efficiently light WIMPs given a positive detection (at the 10% level for $m_\chi \lesssim 50$ GeV), GLAST will be able to confirm and even increase the precision in the case of NFW profile, for a WIMP-nucleon cross-section $\sigma_{\chi-p} \lesssim 10^{-8}$ pb.

Moreover, both XENON and GLAST are complementary with a future ILC project, and the measurements from the three experiments will be able to increase significantly the precision that we can reach on the mass of the WIMP.

Acknowledgements

The authors want to thank particularly G. Bertone for the careful reading of the work. N.B. and A.G. would also like to thank R. K. Singh and A. Djouadi for useful discussions concerning the ILC part of the present work.

Likewise, the authors would like to thank the ENTApP Network of the ILIAS project RII3-CT-2004-506222 and the French ANR project PHYS@COL&COS for financial support.

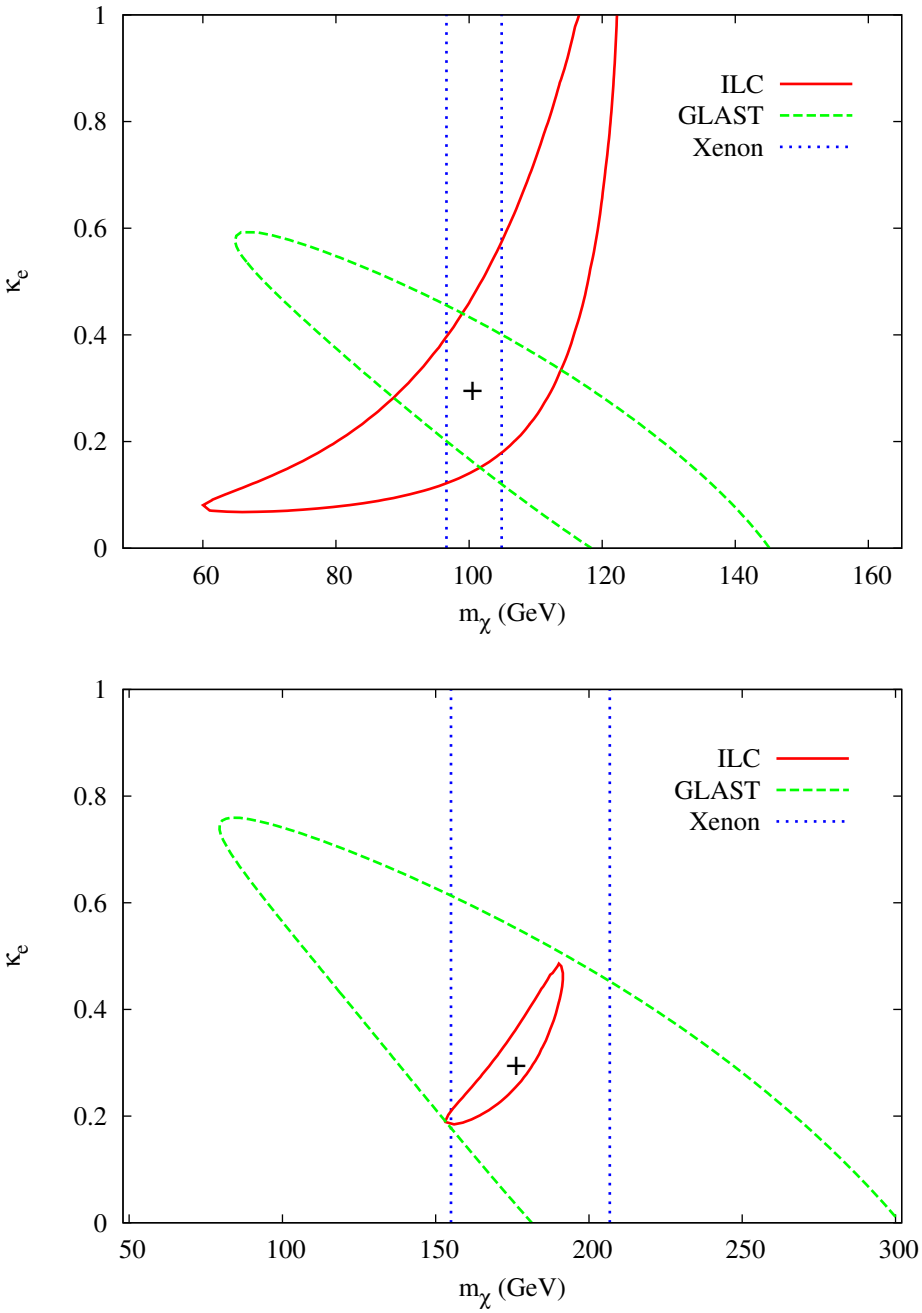

Figure 13: Comparison between a 100 kg XENON-like experiments (dotted line) with $\sigma_{\chi-p} = 10^{-7}$ pb, GLAST (dashed line) in the case of an NFW halo profile with $\langle\sigma v\rangle = 3 \cdot 10^{-26}$ cm^{3}s^{-1}, and unpolarized ILC sensitivity (solid line) at 2σ of confidence level, for different WIMP masses $m_\chi = 100$ and 175 GeV, and $\kappa_e = 0.3$.

Y.M. would like to thanks the members of the Institute for Theoretical Physics of Warsaw for their warm hospitality, and financial support via the "Marie Curie Host Fellowship for Transfer of Knowledge", MTKD-CT-2005-029466. The work of A.G. is sponsored by the hepTOOLS Research Training Network MRTN-CT-2006-035505. The work of C.M. was supported in part by the Spanish DGI of the MEC under Proyectos Nacionales FPA2006-01105 and FPA2006-05423, by the European Union under the RTN programs MRTN-CT-2004-503369 and UniverseNet MRTN-CT-2006-035863, and by the Comunidad de Madrid under Proyecto HEPHACOS S-0505/ESP-0346.

Appendix

In this Appendix we present the method followed in order to obtain the functions describing the standard model particle decay into γ-rays. In order to determine these spectral functions, we generated 300000 events of standard model particles decaying (directly or through secondary decays) into γ-rays using the PYTHIA [30] package, taking care in order to include all possible decay channels. Following the method of Ref. [31] and using the CERNLIB RLSQPM Fortran function, we fitted the resulting spectra through functions of the form:

$$\frac{dN_\gamma^i}{dx} = \exp\left[F_i(\ln(x))\right], \tag{7.23}$$

where i represents the i-th WIMP annihilation channel, $i = WW, ZZ, \text{etc}$; $x = E_\gamma/m_\chi$ with m_χ being the WIMP mass and F are seventh-order polynomial functions which were found to be the following:

$$\begin{aligned}
WW(x) &= -7.72088528 - 8.30185509\,x - 3.28835893\,x^2 - 1.12793422\,x^3 \\
&- 0.266923457\,x^4 - 0.0393805951\,x^5 - 0.00324965152\,x^6 - 0.000113626003\,x^7, \\
ZZ(x) &= -7.67132139 - 7.22257853\,x - 2.0053556\,x^2 - 0.446706623\,x^3 \\
&- 0.0674006343\,x^4 - 0.00639245566\,x^5 - 0.000372241746\,x^6 - 1.08050617\cdot 10^{-5}\,x^7, \\
b\bar{b}(x) &= -11.4735403 - 17.4537277\,x - 11.5219269\,x^2 - 5.1085887\,x^3 \\
&- 1.36697042\,x^4 - 0.211365134\,x^5 - 0.0174275134\,x^6 - 0.000594830839\,x^7, \\
u\bar{u}(x) &= -4.56073856 - 8.13061428\,x - 4.98080492\,x^2 - 2.23044157\,x^3 \\
&- 0.619205713\,x^4 - 0.100954451\,x^5 - 0.00879980996\,x^6 - 0.00031573695\,x^7, \\
d\bar{d}(x) &= -4.77311611 - 10.6317139\,x - 8.33119583\,x^2 - 4.35085535\,x^3 \\
&- 1.33376908\,x^4 - 0.232659817\,x^5 - 0.0213230457\,x^6 - 0.000796017819\,x^7, \\
\tau^-\tau^+(x) &= -5.64725113 - 10.8949451\,x - 7.84473181\,x^2 - 3.50611639\,x^3 \\
&- 0.942047119\,x^4 - 0.14691925\,x^5 - 0.0122521566\,x^6 - 0.000422848301\,x^7.
\end{aligned}$$

The case of WIMP annihilation into e^+e^- or $\mu^+\mu^-$ pairs does not contribute to the photon spectrum (apart from very small contributions in the case of muons, coming from the $\mu \to e^-\bar{\nu}_e\nu_\mu\gamma$ channel, which has a relatively small branching ratio). This means, practically, that the e^+e^- and $\mu^+\mu^-$ spectral functions are set equal to zero. A graphical representation of these functions can be seen in Fig.14.

These functions can afterward be used in order to generate any gamma-ray flux according to eq. (3.6)

As we can see, all contributions are quite similar, apart from the $\tau^-\tau^+$ channel which has a characteristic hard form. Nevertheless, at high energies, the form of all contributions becomes almost identical.

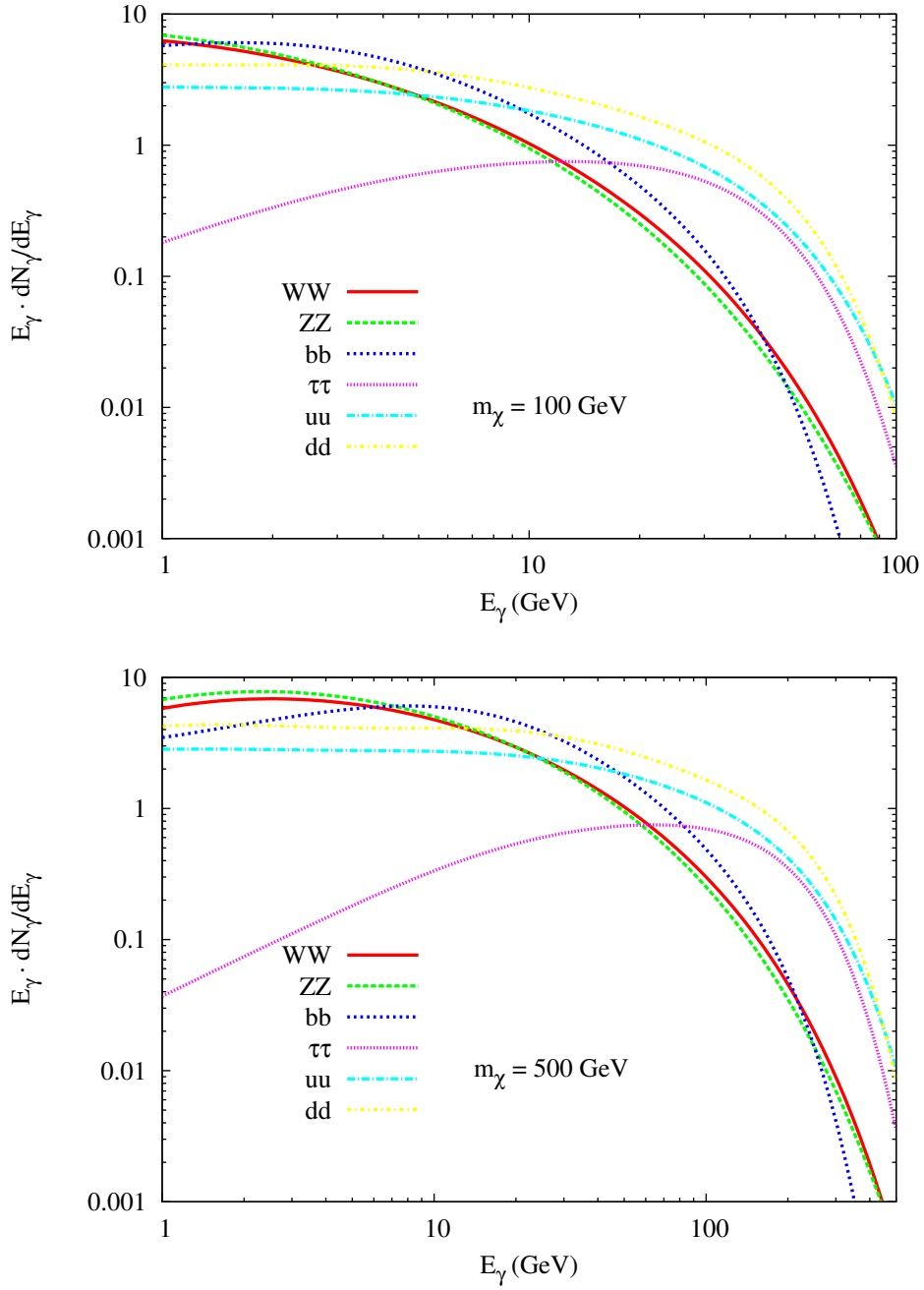

Figure 14: Separate contributions from standard model particles decaying into γ-rays for $m_\chi = 100$ and 500 GeV. The PYTHIA result points have been suppressed for the sake of clarity.

References

[1] For reviews, see: G. Jungman, M. Kamionkowski and K. Griest, Phys. Rept. **267** (1996) 195; C. Munoz, Int. J. Mod. Phys. A **19** (2004) 3093 [arXiv:hep-ph/0309346]; G. Bertone, D. Hooper and J. Silk, Phys. Rept. **405** (2005) 279 [arXiv:hep-ph/0404175].

[2] F. Zwicky, Helv. Phys. Acta **6**, (1933) 110; S. Smith, Astrophys. J. **83** (1936) 23.

[3] J. A. Tyso, G. P. Kochanski and I.P. Dell'Antonio, Astrophys. J. **498**, L107 (1998); D. Clowe, M. Bradac, A. H. Gonzalez, M. Markevitch, S. W. Randall, C. Jones and D. Zaritsky, Astrophys. J. **648** (2006) L109 [arXiv:astro-ph/0608407].

[4] D. N. Spergel *et al.* [WMAP Collaboration], Astrophys. J. Suppl. **170** (2007) 377 [arXiv:astro-ph/0603449]; E. Komatsu *et al.* [WMAP Collaboration], arXiv:0803.0547 [astro-ph].

[5] A. Borriello and P. Salucci, Mon. Not. Roy. Astron. Soc. **323** (2001) 285 [arXiv:astro-ph/0001082].

[6] D. Hooper and E. A. Baltz, arXiv:0802.0702 [hep-ph].

[7] A. M. Green, JCAP **0708** (2007) 022 [arXiv:hep-ph/0703217]; C. L. Shan and M. Drees, arXiv:0710.4296 [hep-ph]; M. Drees and C. L. Shan, arXiv:0803.4477 [hep-ph].

[8] D. Hooper and D. P. Serpico, JCAP **0706**, 013 (2007) [arXiv:astro-ph/0702328]; M. Kachelriess and P. D. Serpico, Phys. Rev. D **76** (2007) 063516 [arXiv:0707.0209 [hep-ph]]; S. Dodelson, D. Hooper and P. D. Serpico, Phys. Rev. D **77** (2008) 063512 [arXiv:0711.4621 [astro-ph]].

[9] J. Angle *et al.* [XENON Collaboration], arXiv:0706.0039 [astro-ph].

[10] N. Gehrels and P. Michelson, *Astropart. Phys.* **11** (1999) 277.

[11] J. F. Navarro, C. S. Frenk and S. D. M. White, *Astrophys. J.* **462** (1996) 563 [arXiv:astro-ph/9508025]; J. F. Navarro, C. S. Frenk and S. D. M. White, *Astrophys. J.* **490** (1997) 493 [arXiv:astro-ph/9611107].

[12] B. Moore, S. Ghigna, F. Governato, G. Lake, T. Quinn, J. Stadel and P. Tozzi, *Astrophys. J.* **524** (1999) L19.

[13] F. Prada, A. Klypin, J. Flix, M. Martinez and E. Simonneau, arXiv:astro-ph/0401512; G. Bertone and D. Merritt, *Mod. Phys. Lett.* **A20** (2005) 1021 [arXiv:astro-ph/0504422]; G. Bertone and D. Merritt, *Phys. Rev.* **D72** (2005) 103502 [arXiv:astro-ph/0501555]; E. Athanassoula, F. S. Ling and E. Nezri, *Phys. Rev.* **D72**, 083503 (2005) [arXiv:astro-ph/0504631].

[14] Y. Mambrini, C. Munoz, E. Nezri and F. Prada, *JCAP* **01** (2006) 010 [arXiv:hep-ph/0506204].

[15] L. Bergstrom, J. Edsjo, P. Gondolo and P. Ullio, Phys. Rev. D **59** (1999) 043506 [astro-ph/9806072].

[16] F. Aharonian et al. [HESS Collaboration], *Astron. Astrophys.* **425** (2004) L13 [arXiv:astro-ph/0408145].

[17] S. Profumo, *Phys. Rev.* **D72** (2005) 103521 [arXiv:astro-ph/0508628]; D. Hooper, I. de la Calle Perez, J. Silk, F. Ferrer and S. Sarkar, *JCAP* **09** (2004) 002 [arXiv:astro-ph/0404205].

[18] F. Aharonian and A. Neronov, *Astrophys. J.* **619** (2005) 306 [arXiv:astro-ph/0408303]; A. Atoyan and C. D. Dermer, *Astrophys. J.* **617** (2004) L123 [arXiv:astro-ph/0410243].

[19] G. Zaharijas and D. Hooper, Phys. Rev. D73 (2006) 103501 [arXiv:astro-ph/0603540].

[20] S. D. Hunger et al. [EGRET Collaboration], *Astrophys. J.* **481** (1997) 205; H. A. Mayer-Hasselwander et al., *Astron. & Astrophys.* **335** (1998) 161.

[21] S. Peirani, R. Mohayaee and J. A. de Freitas Pacheco, Phys. Rev. D **70** (2004) 043503 [arXiv:astro-ph/0401378].

[22] A. Birkedal, K. Matchev and M. Perelstein, Phys. Rev. D **70** (2004) 077701 [arXiv:hep-ph/0403004].

[23] A. Birkedal, AIP Conf. Proc. **805** (2006) 55 [arXiv:hep-ph/0509199].

[24] H. K. Dreiner, O. Kittel and U. Langenfeld, Phys. Rev. D **74**, 115010 (2006) [arXiv:hep-ph/0610020].

[25] H. K. Dreiner, O. Kittel and U. Langenfeld, arXiv:0707.1642 [hep-ph].

[26] A. Pukhov et al., hep-ph/9908288.

[27] A. Pukhov, arXiv:hep-ph/0412191.

[28] C. Bartels and J. List, arXiv:0709.2629 [hep-ex].

[29] J. L. Feng, S. Su and F. Takayama, Phys. Rev. Lett. **96** (2006) 151802 [arXiv:hep-ph/0503117].

[30] T. Sjostrand, S. Mrenna and P. Skands, JHEP **0605** (2006) 026 [arXiv:hep-ph/0603175].

[31] J. Hisano, S. Matsumoto, O. Saito and M. Senami, Phys. Rev. D **73** (2006) 055004 [arXiv:hep-ph/0511118].